



UNIVERSITÀ
DEGLI STUDI
FIRENZE

FLORE

Repository istituzionale dell'Università degli Studi di Firenze

Mesoscopic optical imaging of whole mouse heart

Questa è la Versione finale referata (Post print/Accepted manuscript) della seguente pubblicazione:

Original Citation:

Mesoscopic optical imaging of whole mouse heart / Giardini F.; Lazzeri E.; Olianti C.; Beconi G.; Costantini I.; Silvestri L.; Cerbai E.; Pavone F.S.; Sacconi L.. - In: JOURNAL OF VISUALIZED EXPERIMENTS. - ISSN 1940-087X. - ELETTRONICO. - 2021:(2021), pp. 0-0. [10.3791/62795]

Availability:

This version is available at: 2158/1260658 since: 2022-05-06T16:26:20Z

Published version:

DOI: 10.3791/62795

Terms of use:

Open Access

La pubblicazione è resa disponibile sotto le norme e i termini della licenza di deposito, secondo quanto stabilito dalla Policy per l'accesso aperto dell'Università degli Studi di Firenze (<https://www.sba.unifi.it/upload/policy-oa-2016-1.pdf>)

Publisher copyright claim:

Conformità alle politiche dell'editore / Compliance to publisher's policies

Questa versione della pubblicazione è conforme a quanto richiesto dalle politiche dell'editore in materia di copyright.

This version of the publication conforms to the publisher's copyright policies.

(Article begins on next page)

1 **Authors' version –**
2 **Published source** Giardini, F., Lazzeri, E., Olianti, C., Beconi, G., Costantini, I., Silvestri, L., Cerbai,
3 **E., Pavone, F. S., Sacconi, L. Mesoscopic Optical Imaging of Whole Mouse Heart. J. Vis.**
4 **Exp. (176), e62795, doi:10.3791/62795 (2021).**

5 **LINK to Published version** [https://www.jove.com/it/t/62795/mesoscopic-optical-imaging-of-](https://www.jove.com/it/t/62795/mesoscopic-optical-imaging-of-whole-mouse-heart)
6 [whole-mouse-heart](https://www.jove.com/it/t/62795/mesoscopic-optical-imaging-of-whole-mouse-heart)

7 **Copyright: Journal of Visualized Experiments**

8
9
10 **TITLE:**

11 Mesoscopic Optical Imaging of Whole Mouse Heart

12
13 **AUTHORS AND AFFILIATIONS:**

14 Francesco Giardini^{1,*}, Erica Lazzeri^{1,*}, Camilla Olianti^{1,*}, Giada Beconi¹, Irene Costantini^{1,2}, Ludovico
15 Silvestri^{1,3,4}, Elisabetta Cerbai^{1,5}, Francesco S. Pavone^{1,3,4}, Leonardo Sacconi^{1,3,#}

16
17 ¹European Laboratory for Non-Linear Spectroscopy, Sesto Fiorentino, 50019, Italy.

18 ²Department of Biology, University of Florence, Sesto Fiorentino, 50019, Italy.

19 ³National Institute of Optics, National Research Council, Florence, 50125, Italy.

20 ⁴Department of Physics and Astronomy, University of Florence, Sesto Fiorentino, 50019, Italy.

21 ⁵Department of Neurosciences, Psychology, Drugs and Child Health, University of Florence, Italy.

22
23 * The authors contributed equally to the work.

24
25 Email addresses of co-authors:

26 Francesco Giardini (giardini@lens.unifi.it)

27 Erica Lazzeri (lazerierica@gmail.com)

28 Camilla Olianti (olianti@lens.unifi.it)

29 Giada Beconi (giada.beconi@gmail.com)

30 Irene Costantini (costantini@lens.unifi.it)

31 Ludovico Silvestri (silvestri@lens.unifi.it)

32 Elisabetta Cerbai (cerbai@lens.unifi.it)

33 Francesco S. Pavone (pavone@lens.unifi.it)

34 Leonardo Sacconi (sacconi@lens.unifi.it)

35
36 #Corresponding author:

37 Leonardo Sacconi (sacconi@lens.unifi.it)

38
39 **SUMMARY:**

40 We report a method for mesoscopic reconstruction of the whole mouse heart by combining new
41 advancements in tissue transformation and staining with the development of an axially scanned
42 light-sheet microscope.

43
44 **ABSTRACT:**

45 Both genetic and non-genetic cardiac diseases can cause severe remodeling processes in the heart.
46 Structural remodeling, such as collagen deposition (fibrosis) and cellular misalignment, can affect
47 electrical conduction, introduce electromechanical dysfunctions and, eventually lead to arrhythmia.
48 Current predictive models of these functional alterations are based on non-integrated and low-
49 resolution structural information. Placing this framework on a different order of magnitude is

50 challenging due to the inefficacy of standard imaging methods in performing high-resolution imaging
51 in massive tissue. In this work, a new methodological framework is described that allows imaging of
52 whole mouse hearts with micrometric resolution. The achievement of this goal has required an
53 impressive technological effort where advances in tissue transformation and imaging methods have
54 been combined. First, we describe an optimized CLARITY protocol capable of transforming an intact
55 heart into a nanoporous, hydrogel-hybridized, lipid-free form that allows high transparency and
56 deep staining is described. Then, a fluorescence light-sheet microscope able to rapidly acquire
57 images of a mesoscopic field of view (mm-scale) with the micron-scale resolution is described.
58 Inspired by the mesoSPIM project, the conceived microscope allows the reconstruction of the whole
59 mouse heart with micrometric resolution in a single tomographic scan. We believe that this
60 methodological framework will allow clarifying the involvement of the cytoarchitecture disarray in
61 the electrical dysfunctions and pave the way for a comprehensive model that considers both the
62 functional and structural data, thus enabling a unified investigation of the structural causes that lead
63 to the electrical and mechanical alterations after the tissue remodeling.
64

65 **INTRODUCTION:**

66 Structural remodeling associated with cardiac diseases can affect electrical conduction and
67 introduce electromechanical dysfunctions of the organ^{1,2}. Current approaches used to predict
68 functional alterations commonly employ MRI and DT-MRI to obtain an overall reconstruction of
69 fibrosis deposition, vascular tree, and fiber distribution of the heart, and they are used to model
70 preferential action potential propagation (APP) paths across the organ^{3,4}. These strategies can
71 provide a beautiful overview of the heart organization. However, their spatial resolution is
72 insufficient to investigate the impact of structural remodeling on cardiac function at the cellular
73 level.
74

75 Placing this framework at a different order of magnitude, where single cells can play individual roles
76 on action potential propagation, is challenging. The main limitation is the inefficiency of standard
77 imaging methods to perform high-resolution imaging (micrometric resolution) in massive
78 (centimeter-sized) tissues. In fact, imaging biological tissues in 3D at high resolution is very
79 complicated due to tissue opaqueness. The most common approach to perform 3D reconstructions
80 in entire organs is to prepare thin sections. However, precise sectioning, assembling, and imaging
81 require significant effort and time. An alternative approach that does not demand cutting the sample
82 is to generate a transparent tissue. During the last years, several methodologies for clarifying tissues
83 have been proposed⁵⁻⁸. The challenge to produce massive, transparent, and fluorescently-labeled
84 tissues has been recently achieved by developing true tissue transformation approaches (CLARITY⁹,
85 SHIELD¹⁰). In particular, the CLARITY method is based on the transformation of an intact tissue into
86 a nanoporous, hydrogel-hybridized, lipid-free form that enables to confer high transparency by the
87 selective removal of membrane lipid bilayers. Notably, this method has been found successful also
88 in cardiac preparation¹¹⁻¹⁴. However, since the heart is too fragile to be suitable for an active clearing,
89 it must be cleared using the passive approach, which requires a long time to confer complete
90 transparency.
91

92 In combination with advanced imaging techniques like light-sheet microscopy, CLARITY has the
93 potential to image 3D massive heart tissues at micrometric resolution. In light-sheet microscopy, the
94 illumination of the sample is performed with a thin sheet of light confined in the focal plane of the
95 detection objective. The fluorescence emission is collected along an axis perpendicular to the
96 illumination plane¹⁵. The detection architecture is similar to widefield microscopy, making the
97 acquisition much faster than laser scanning microscopes. Moving the sample through the light sheet
98 permits obtaining a complete tomography of big specimens, up to centimeter-sized samples.

99 However, due to the intrinsic properties of the Gaussian beam, it is possible to obtain a very thin (of
100 the order of a few microns) light-sheet only for a limited spatial extension, thus drastically limiting
101 the field of view (FoV). Recently, a novel excitation scheme has been introduced to overcome this
102 limitation and applied for brain imaging, allowing 3d reconstructions with isotropic resolution¹⁶.

103
104 In this paper, a passive clearing approach is presented, enabling a significant reduction of the
105 clearing timing needed by the CLARITY protocol. The methodological framework described here
106 allows reconstructing a whole mouse heart with micrometric resolution in a single tomographic scan
107 with an acquisition time in the order of minutes.

108 109 **PROTOCOL:**

110
111 All animal handling and procedures were performed in accordance with the guidelines from
112 Directive 2010/63/EU of the European Parliament on the protection of animals used for scientific
113 purposes and conformed to the principles and regulations of the Italian Ministry of Health. The
114 experimental protocol was approved by the Italian Ministry of Health (protocol number 647/2015-
115 PR). All the animals were provided by ENVIGO, Italy. For these experiments, 5 male C57BL/6J mice
116 of 6 months of age were used.

117 118 **1. Solution preparation**

119
120 1.1. Prepare 4% Paraformaldehyde (PFA) in Phosphate-Buffered Saline (PBS) (pH 7.6) in a chemical
121 hood. Store the 4% PFA aliquots at -20 °C for several months.

122
123 1.2. Prepare Hydrogel solution: Mix 4% Acrylamide, 0.05% Bis-acrylamide, 0.25% Initiator AV-044 in
124 0.01 M PBS in a chemical hood. Keep the reagents and the solution on ice during the entire
125 preparation. Store the hydrogel aliquots at -20 °C for several months.

126
127 1.3. Prepare Clearing solution: Mix 200 mM Boric acid, 4% Sodium Dodecyl-Sulfate (SDS) in deionized
128 water; pH 8.6 in a chemical hood. Store the solution between 21–37 °C to avoid SDS precipitation.

129
130 1.4. Prepare fresh Tyrode solution on the day of the experiment: Add 10 mM Glucose, 10 mM HEPES,
131 113 mM NaCl, 1.2 mM MgCl₂, and 4.7 mM KCl; titrate to pH 7.4 using 1 M NaOH.

132 133 **2. Heart isolation**

134
135 2.1. Inject 0.1 mL of 500 I.U. Heparin subcutaneously 30 min before the heart isolation procedure.

136
137 2.2. Fill a 30-mL syringe and three 6-cm Petri dishes with fresh Tyrode solution. Make a small rift (3–
138 4 mm in depth) on the border of one of the Petri dishes and place it under a stereoscopic microscope.

139
140 2.3. Fix a 1 mm-diameter cannula to the syringe and insert it in the rift of the Petri dish. Make sure
141 there are no air bubbles in the syringe.

142
143 2.4. Fill a 20-mL syringe with 4% PFA and keep it in the chemical hood. Prepare an empty Petri dish
144 under the hood.

145
146 2.5. Anesthetize the mouse with 3% Isoflurane/oxygen at a flow rate of 1.0 L/min and sacrifice it by
147 cervical dislocation according to animal welfare rules in force.

148
149 2.6. After the sacrifice, remove the fur over the chest and open the chest to have full access to the
150 heart.
151
152 2.7. Isolate the heart, immerse it in the Petri dish previously filled with 50 mL of Tyrode Solution.
153 Use surgical scissors to cut the aorta immediately near the aortic arch to have the heart exposed.
154
155 2.8. Transfer the heart under a stereoscopic microscope and carefully perform the cannulation. Do
156 not insert the cannula too deep into the aorta (no more than 2 mm) to avoid tissue damage.
157
158 2.9. Use a little clamp and a suture (size 5/0) to fix the heart to the cannula.
159
160 2.10. Perfuse the heart with 30 mL of the Tyrode solution with a constant pressure of 10 mL/min to
161 remove blood from the vessels.
162
163 2.11. Detach the cannula from the syringe and place the heart in the Petri dish filled with Tyrode
164 solution. Be careful not to have air bubbles in the cannula; otherwise, remove the air bubbles
165 properly.
166
167 2.12. Attach the 20-mL syringe filled with cold 4% PFA to the cannula and perfuse the heart at the
168 same constant pressure.
169
170 2.13. Incubate the heart in 10 mL of 4% PFA at 4 °C overnight (O/N). To avoid tissue degradation,
171 perform steps 2.6–2.13 in the shortest time possible.
172

173 **3. Heart clearing**
174

175 3.1. The following day, wash the heart in 0.01 M PBS 3 times at 4 °C for 15 min.
176

177 NOTE: After this step, the heart can be stored in PBS + 0.01% sodium azide (NaN₃) at 4 °C for several
178 months.
179

180 3.2. Incubate the heart in 30 mL of Hydrogel solution in shaking (15 rpm) at 4 °C for 3 days.
181

182 3.3. Degas the sample at room temperature using a dryer, a vacuum pump, and a tube system that
183 connects the dryer to both the pump and a nitrogen pipeline.
184

185 3.3.1. Place the sample in the dryer and open the vial, keeping the cap on it.
186

187 3.3.2. Close the dryer and remove the oxygen from the tube by opening the nitrogen pipeline.
188

189 3.3.3. Turn on the vacuum pump to remove the oxygen from the dryer for 10 min.
190

191 3.3.4. Turn off the pump and use the knob of the dryer to open the nitrogen pipeline. Once the
192 pressure is equal to the atmospheric pressure, carefully open the dryer and quickly close the vial.
193

194 3.4. Keep the heart in the degassed Hydrogel solution at 37 °C for 3 h at rest.
195

196 3.5. When the Hydrogel is properly polymerized and appears entirely gelatinous, carefully remove
197 the heart from it and place it in the sample holder.

198
199 3.6. Insert the sample holder with the heart in one of the clearing chambers and close it properly to
200 avoid leaks of the clearing solution.

201
202 3.7. Switch on the water bath where the clearing solution container is placed and the peristaltic
203 pump to start the recirculation of the clearing solution.

204
205 3.8. Change the clearing solution in the container once a week to speed up the clarification
206 procedure.

207 208 **4. Cellular membrane staining**

209
210 4.1. Once the heart appears completely clarified, remove it from the sample holder and wash it in
211 50 mL of warmed-up PBS for 24 h. Wash again in 50 mL of PBS + 1% of Triton-X (PBS-T 1x) for 24 h.

212
213 4.2. Incubate the sample in 0.01 mg/mL Wheat Germ Agglutinin (WGA) – Alexa Fluor 633 in 3 mL of
214 PBS-T 1x in shaking (50 rpm) at room temperature for 7 days.

215
216 4.3. After the 7-day incubation, wash the sample in 50 mL of PBS-T 1x at room temperature in
217 shaking for 24 h.

218
219 4.4. Incubate the sample in 4% PFA for 15 min and then wash it 3 times in PBS for 5 min each.

220
221 NOTE: After this step, the heart can be stored in PBS + 0.01% NaN₃ at 4 °C for several months.

222
223 4.5. Incubate the heart in increasing concentrations of 2,2'-Thiodiethanol (TDE) in 0.01 M PBS (20%
224 and 47% TDE/PBS) for 8 h each, up to the final concentration of 68% TDE in 0.01 M PBS to provide
225 the required refractive index (RI = 1.46). This is the RI matching medium (RI-medium) to acquire
226 images¹⁶.

227 228 **5. Heart mounting and acquisition**

229
230 NOTE: All the components of the optical system are listed in detail in the **Table of Materials**.

231
232 5.1. Gently fill about 80% of the external cuvette (quartz, 45 mm × 45 mm × 42.5 mm) with the RI-
233 medium.

234
235 NOTE: Here, it is possible to use different non-volatile solutions that guarantee a RI of 1.46.

236
237 5.2. Gently fill the internal cuvette (quartz, 45 mm × 12.5 mm × 12.5 mm) with the same RI-medium.

238
239 5.3. Immerse the sample inside the internal cuvette. The sample incubations described above allow
240 the sample to remain stable inside the RI-medium without being held.

241
242 5.4. Gently move the sample to the bottom of the cuvette using thin tweezers and arrange the heart
243 with its longitudinal axis parallel to the cuvette's main axis to minimize the excitation light path
244 across the tissue during the scanning.

- 245
246 5.5. Gently fix the tailored plug above the internal cuvette with two screws.
247
248 5.6. Mount the sample to the microscope stage using the magnets.
249
250 5.7. Translate the vertical sample stage manually to immerse the internal cuvette into the external
251 one.
252
253 5.8. Turn on the excitation light source (wavelength of 638 nm), setting a low power (in the order of
254 3 mW).
255
256 5.9. Move the sample using the motorized translator to illuminate an inner plane of the tissue.
257
258 5.10. Turn on the imaging software (HCImageLive) and set the camera **Trigger** on **External Edge**
259 **Trigger (light-sheet)** mode to drive the acquisition trigger of the camera by the custom software
260 controlling the entire setup.
261
262 5.11. Enable **Autosave** in the **Scan Settings** panel and set the output folder where the images need
263 to be saved.
264
265 5.12. Manually adjust the sample position in the XY plane with the linear translators to move the
266 sample to the center of the FoV of the camera sensor.
267
268 5.13. Move the sample along the Z-axis using the linear motorized translator to identify heart
269 borders for tomographic reconstruction.
270
271 5.14. Increase the laser power to ~20 mW, ready for the imaging session.
272
273 5.15. Start the tomographic acquisition, click the **Start** button in the **Capture** panel of the imaging
274 software, and at the same time move the sample along the Z-axis at the constant velocity of 6 $\mu\text{m/s}$
275 using the motorized translator.
276

277 **REPRESENTATIVE RESULTS:**

278 The developed passive clearing setup allows to obtain a cleared adult mouse heart (with a dimension
279 of the order 10 mm x 6 mm x 6 mm) in about 3 months. All the components of the setup are
280 mounted, as shown in **Figure 1**. The negligible temperature gradient between each clearing chamber
281 (of the order of 3°C) allows maintaining the temperature in a proper range across all chambers.
282

283 [insert **Figure 1** here]
284

285 **Figure 2** shows the result of the clearing process of an entire heart. As already reported by Costantini
286 et al.¹⁶, the combination of the CLARITY methodology with TDE as RI-medium does not significantly
287 change the sample's final volume nor leads to anisotropic deformation of the specimen.
288

289 [insert **Figure 2** here]
290

291 Once the heart was cleared, cellular membranes were stained with an Alexa Fluor 633-conjugated
292 WGA to perform the cytoarchitecture reconstruction of the entire organ. The custom-made

293 fluorescence light-sheet microscope (**Figure 3**) was able to ensure 3D micron-scale resolution across
294 the entire FoV.

295
296 [insert **Figure 3** here]

297
298 Considering the numerical aperture ($NA = 0.1$) of the detection optics, the radial (XY) Point Spread
299 Function (PSF) of the system can be estimated in the order of 4–5 μm . On the other hand, the
300 excitation optics produce a light-sheet with a minimum waist of about 6 μm (Full width half
301 maximum, FWHM) that diverges up to 175 μm at the edge of the FoV (**Figure 4A–C**). The
302 synchronization of the camera rolling shutter with the axial scan of the light-sheet waist ensures to
303 excite the sample with the thinnest portion of the light-sheet, resulting in an average FWHM of about
304 6.7 μm along the entire FoV (**Figure 4B–D**).

305
306 [insert **Figure 4** here]

307
308 The Z-PSF of the microscope was also estimated by a tomographic reconstruction of the fluorescent
309 nanosphere (**Figure 5**). An FWHM of 6.4 μm can be estimated by the fit, in good agreement with the
310 previous assessment.

311
312 [insert **Figure 5** here]

313
314 Owing to the high transparency of the tissue, it was possible to illuminate the whole heart without
315 significant distortion of the axially scanned light-sheet at an excitation wavelength of 638 nm. The
316 fluorescence signal was collected by the sCMOS sensor operating at 500 ms of exposure time and a
317 frame rate of 1.92 Hz. Based on previous quantification, the tomographic acquisition was performed
318 using a Z-scan velocity of 6 $\mu\text{m}/\text{s}$, and assuming a frame rate of 1.92 Hz, one frame every 3.12 μm
319 was acquired, oversampling the system Z-PSF by about two times. Two representative frames (on
320 the coronal and transverse planes) of the left ventricle chamber are shown in **Figure 6**. This result
321 confirms the potentiality of the system to resolve single cellular membranes in three dimensions
322 with a sufficient Signal/Noise ratio in the entire organ (**Figure 6**).

323
324 [insert **Figure 6** here]

325 326 **FIGURE AND TABLE LEGENDS:**

327 **Figure 1: Schematic of the passive clearing setup.** The clearing solution (after being filtered)
328 circulates in succession through the sample chambers with the help of the peristaltic pump. The
329 maintenance of the solution container in a water bath set at 50 °C allows the solution temperature
330 to be between 37–45 °C within the chambers. Image created with Biorender.com.

331
332 **Figure 2: Representative image of a heart before (on the left) and after (on the right) the CLARITY**
333 **protocol.** The hearts become fully transparent and slightly oversized.

334
335 **Figure 3: MesoSPIM.** CAD renderings of the custom-made fluorescence light-sheet microscope.

336
337 **Figure 4: Light-sheet generation and characterization. (A)** An excitation light-sheet generated with
338 a laser source of 638 nm is focused on the center of the Field of View (FoV) and acquired with a pixel
339 size of 3.25 μm and an Exposure Time of 10 ms. Light intensity is normalized and reported with a
340 colormap. The Full Width Half Maximum (FWHM) of the light intensity profile is evaluated in 15
341 different positions along the FoV. Results are shown in **C**. **(B)** Image of the excitation light-sheet

342 generated by the synchronization between the camera rolling shutter operating at 1.92 Hz and the
343 light beam position driven by the tunable lens. The FWHM of the light intensity profile is evaluated
344 along the FoV and results are shown in **D**.

345
346 **Figure 5: Point Spread Function in the Z-axis.** The Point Spread Function (PSF) of the optical system
347 is estimated by imaging fluorescent sub-micron-scale nanospheres (excited with a light sheet with a
348 wavelength of 638 nm) with a pixel size of $3.25 \mu\text{m} \times 3.25 \mu\text{m} \times 2.0 \mu\text{m}$. PSF intensity profile along
349 the optical axis (Z) is represented as black dots. PSF profile is fitted with a Gaussian function with μ
350 $= 18.6 \mu\text{m}$ and $\sigma = 2.7 \mu\text{m}$. The FWHM of the PSF estimated by the fit is $6.4 \mu\text{m}$.

351
352
353 **Figure 6: Mouse heart tissue reconstruction.** The clarified heart was stained with WGA conjugated
354 to Alexa Fluor 633 and excited by a laser source with a wavelength of 638 nm. **(A)** Coronal and **(B)**
355 transverse representative sections. **(C–D)** Tissue transformation produces high tissue transparency,
356 allowing to resolve small structures in the wall depth. The optical system shows an axial resolution
357 sufficient to resolve micrometric structures (panel. **D**). **(E)** 3D low-resolution heart rendering.

358 359 **DISCUSSION:**

360 In this work, a successful approach to clear, stain, and image a whole mouse heart at high resolution
361 was introduced. First, a tissue transformation protocol (CLARITY) was optimized and performed,
362 slightly modified for its application on the cardiac tissue. Indeed, to obtain an efficient
363 reconstruction in 3D of a whole heart, it is essential to prevent the phenomenon of light scattering.
364 The CLARITY methodology allows us to obtain a highly transparent intact heart, but it requires long
365 incubation times when performed passively (about 5 months). With respect to the brain, the cardiac
366 tissue is not suitable for an active clearing, which takes advantage of an electric field. Even at low
367 voltages, the electric field leads to damages and tissue breakages. Here, a passive clearing approach
368 was optimized to obtain a completely cleared heart in about 3 months. After isolating and
369 cannulating the heart through the proximal aorta, the CLARITY methodology was performed as
370 described in section 3 of the protocol. To speed up the procedure, a homemade passive clearing
371 setup was arranged (**Figure 1**), which ended up decreasing the timing of tissue clearing by about
372 40%. The setup is composed of a container for the clearing solution, a water bath, a peristaltic pump,
373 several chambers containing different sample holders, capsule filters for each chamber, and a tubing
374 system for the recirculation of the solution. The pump extracts and circulates the solution from the
375 container in succession through each of the chambers, where the samples are held for clearing.
376 Before entering the chambers, the solution flows through a capsule filter to trap the lipids flushed
377 away from tissues during the clearing. The optimal temperature for the clearing solution, between
378 $37\text{--}45 \text{ }^\circ\text{C}$, is maintained within the chambers during the recirculation by keeping the solution
379 container in a water bath at $50 \text{ }^\circ\text{C}$. It is advised to change the clearing solution in the container once
380 a week during the procedure. All components used are listed in detail in the **Table of Materials**. The
381 optimized solution presented here allows us to obtain a whole passively cleared mouse heart in a
382 significantly shorter time with respect to the standard passive clearing technique, thus reducing the
383 required experimental time without damaging the organ. The staining approach was also optimized
384 for homogeneous labeling of the cellular membranes and endothelium, using a fluorescent lectin
385 (WGA – Alexa Fluor 633).

386
387 The heart cytoarchitecture has been reconstructed by developing a dedicated mesoSPIM that axially
388 sweeps the light-sheet across the sample (<https://mesospim.org>). The custom-made fluorescence
389 light-sheet microscope (**Figure 3**) was able to rapidly acquire images of a mesoscopic FoV (of the
390 order of millimeters) with micrometric resolution. In this way, single cardiomyocytes can be resolved

391 and mapped into a 3D reconstruction of the entire organ. The microscope illuminates the cleared
392 sample with a light-sheet, dynamically generated by scanning a laser beam at 638 nm using a
393 galvanometric mirror. A sCMOS camera characterizes the detection arm in a 2x magnification
394 scheme which enables it to acquire the entire FoV in a single scan. The fluorescence signal was
395 selected by placing a long-pass filter after the objective. The camera was set to work in rolling shutter
396 mode: at any time, the line of active camera pixels (i.e., exposed to the image) is synchronized with
397 the in-plane shift of the focal band of the light-sheet, performed by an electrically tunable lens. This
398 approach maximized the optical sectioning capability in the whole FoV by only acquiring images in
399 the thinnest part of the focused light-sheet. This solution differs from conventional configurations,
400 where acquisition involves the entire range of focal depth of the light-sheet, preventing peak optical
401 sectioning resolution in large part of the FoV. An integrated sample stage supports cuvettes, thereby
402 optimizing positioning and enabling axial movement of the sample during the imaging process. In
403 this way, tomographic reconstructions are possible by acquiring consecutive internal sections. The
404 images obtained have a mesoscopic FoV and a micrometric resolution, while the acquisition time
405 required for a whole mouse heart is ~ 15 min. The synchronization between the camera rolling
406 shutter and the excitation light beam sweeping the FoV allows acquiring the entire image plane with
407 a high spatial resolution (**Figure 4**). This allows direct reconstruction of the sample in a single
408 tomographic acquisition, without the necessity of sample radial displacement and multi-adjacent-
409 stacks-based imaging. Notably, the microscope allowed the reconstruction of the entire organ of
410 about (10 mm x 6 mm x 6 mm) in a single imaging session, with a near-isotropic voxel size and a
411 sufficient signal-to-background ratio to resolve single cells across the whole organ potentially.

412
413 It is noteworthy that the proposed protocol presents some critical steps that must be performed
414 carefully to achieve good results. In particular, the cannulation of the heart through the proximal
415 aorta can be quite difficult, but it is an essential step to wash and fix the organ properly. Judd et al.¹⁷,
416 showed how to perform this step effectively. Moreover, the degassing procedure needed by the
417 CLARITY protocol is quite complex too, but it is essential for tissue preservation; if this step is not
418 performed properly, the tissue could encounter damages and decay during the incubation in clearing
419 solution.

420
421 Furthermore, although the presented experimental workflow is suitable for small fluorescent
422 probes, the use of immunohistochemistry does not always provide good efficiency in the staining
423 due to the higher molecular weight of the antibodies. Each immunostaining protocol requires proper
424 optimization, and different approaches have been conceived to improve the antibody penetration,
425 for example, tissue expansion¹⁸ and/or variations in pH and ionic strength¹⁹.

426
427 The mesoSPIM setup also presents two main limitations: i) the light-sheet preservation across the
428 sample is strongly dependent on the tissue transparency, and ii) the dimension of the camera sensor
429 limits the FoV. Guaranteeing a perfect refractive index matching inside the entire heart is very
430 challenging, and small variations on the refractive index can produce light scattering, leading to
431 degradation of the image quality. In this respect, a dual-side illumination scheme can be introduced.
432 Two excitation arms can generate two distinct and aligned dynamic light sheets with maximally
433 focused illumination by alternating the illumination from one side to the other of the specimen.
434 Also, the FoV can be improved by using a new generation high-resolution back-illuminated sCMOS
435 with very large sensors in combination with high numerical aperture telecentric lenses with low field
436 distortion. This implementation would allow us to reconstruct bigger organs or expanded tissues
437 maintaining the same optical section capability and thus producing micron-scale 3D images of
438 centimeter-sized cleared samples.

439

440 Although the presented protocol still requires a long time for sample preparation and a high level of
441 transparency to obtain a reliable cytoarchitecture reconstruction of the entire organ, the main
442 significance of the approach resides in the improvements of the clearing protocol and the capability
443 to perform mesoscopic reconstruction in a single scan at micrometric resolution. In the future, these
444 advances can be combined with a multi-staining protocol to achieve whole-organ reconstruction
445 integrating different biological structures.

446

447 **ACKNOWLEDGMENTS:**

448 This project has received funding from the European Union's Horizon 2020 research and innovation
449 program under grant agreement No 95216.

450

451 **DISCLOSURES:**

452 Nothing to disclosure.

453

454 **REFERENCES:**

- 455 1. Cohn, J. N., Ferrari, R., Sharpe, N. Cardiac remodeling-concepts and clinical implications: A
456 consensus paper from an International Forum on Cardiac Remodeling. *Journal of the American*
457 *College of Cardiology*. **35**, 569–582 (2000).
- 458 2. Finocchiaro, G. et al. Arrhythmogenic potential of myocardial disarray in hypertrophic
459 cardiomyopathy: genetic basis, functional consequences and relation to sudden cardiac death. *EP*
460 *Europace*. **2**, 1–11 (2021).
- 461 3. Bishop, M. J. et al. Development of an anatomically detailed MRI-derived rabbit ventricular
462 model and assessment of its impact on simulations of electrophysiological function. *American*
463 *Journal of Physiology – Heart and Circulatory Physiology*. **298** (2), H699–H718 (2010).
- 464 4. Bishop, M. J., Boyle, P. M., Plank, G., Welsh, D. G., Vigmond, E. J. Modelling the role of the
465 coronary vasculature during external field stimulation. *IEEE Transaction on Biomedical Engineering*.
466 **57**, 2335–2345 (2010).
- 467 5. Tainaka, K. et al. Whole-body imaging with single-cell resolution by tissue decolorization.
468 *Cell*. **159**, 911–924 (2014).
- 469 6. Ueda, H. R. et al. Whole-brain profiling of cells and circuits in mammals by tissue clearing
470 and light-sheet microscopy. *Neuron* **106**, 369–387 (2020).
- 471 7. Richardson, D. S., Lichtman, J. W. Clarifying tissue clearing. *Cell*. **162**, 246–257 (2015).
- 472 8. Silvestri, L., Costantini, I., Sacconi, L., Pavone, F. S. Clearing of fixed tissue: a review from a
473 microscopist's perspective. *Journal of Biomedical Optics*. **21**, 081205 (2016).
- 474 9. Chung, K. et al. Structural and molecular interrogation of intact biological systems. *Nature*.
475 **497**, 332–337 (2013).
- 476 10. Park, Y. G. et al. Protection of tissue physicochemical properties using polyfunctional
477 crosslinkers. *Nature Biotechnology*. **37**, 73 (2019).
- 478 11. Ding, Y. et al. Light-sheet fluorescence microscopy for the study of the murine heart.
479 *Journal of Visualized Experiments: JoVE*. **139**, 57769 (2018).
- 480 12. Olianti, C. et al. 3D imaging and morphometry of the heart capillary system in
481 spontaneously hypertensive rats and normotensive controls. *Scientific Reports*. **10**, 1–9 (2020).
- 482 13. Pianca, N. et al. Cardiac sympathetic innervation network shapes the myocardium by locally
483 controlling cardiomyocyte size through the cellular proteolytic machinery. *The Journal of*
484 *Physiology*. **597**, 3639–3656 (2019).
- 485 14. Di Bona, A., Vita, V., Costantini, I., Zaglia, T. Towards a clearer view of sympathetic
486 innervation of cardiac and skeletal muscles. *Progress in Biophysics and Molecular Biology* **154**, 80–
487 93 (2020).

- 488 15. Voigt, F. F. et al. The mesoSPIM initiative – open-source light-sheet microscopes for imaging
489 cleared tissue. *Nature Methods*. **16** (11), 1105–1108 (2019).
490 16. Costantini, I. et al. A versatile clearing agent for multi-modal brain imaging. *Scientific*
491 *Reports*. **5**, 9808 (2015).
492 17. Judd, J., Lovas, J., Huang, G. N. Isolation, culture and transduction of adult mouse
493 cardiomyocytes. *Journal of Visualized Experiments: JoVE*. **114**, 54012 (2016).
494 18. Yi, F. et al. Microvessel prediction in H&E stained pathology images using fully convolutional
495 neural networks. *BMC Bioinformatics*. **19** (1), 64 (2018).
496 19. Susaki, E. A. et al. Versatile whole-organ/body staining and imaging based on electrolyte-gel
497 properties of biological tissues. *Nature Communications*. **11** (1), 1982 (2020).
498
499

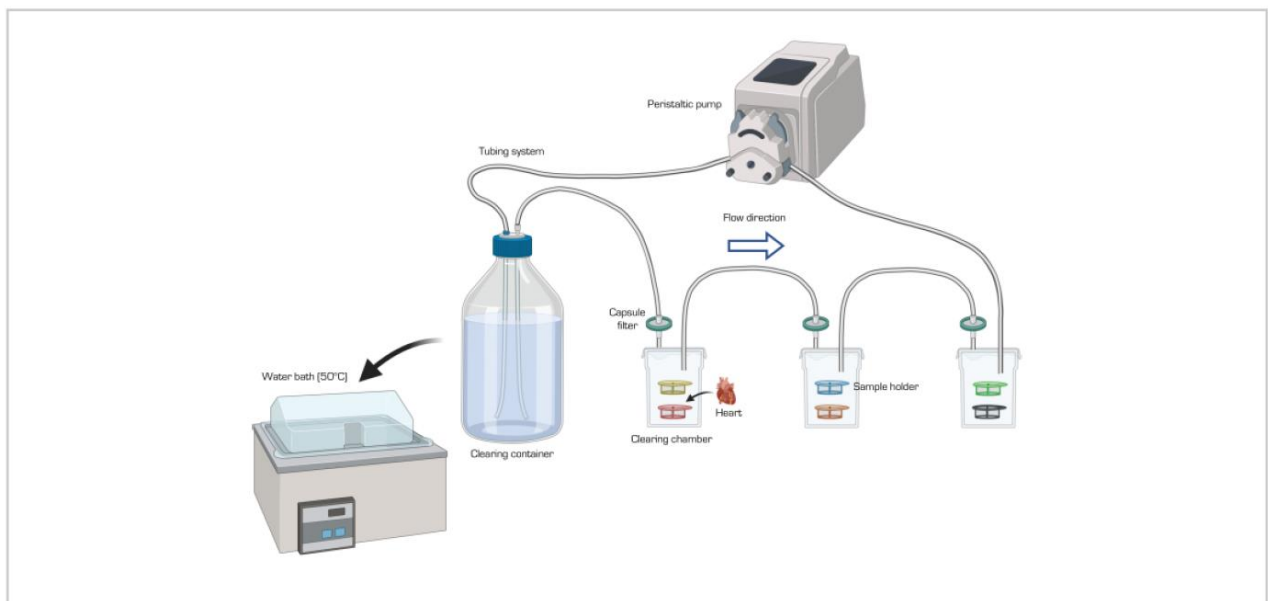


Figure 1

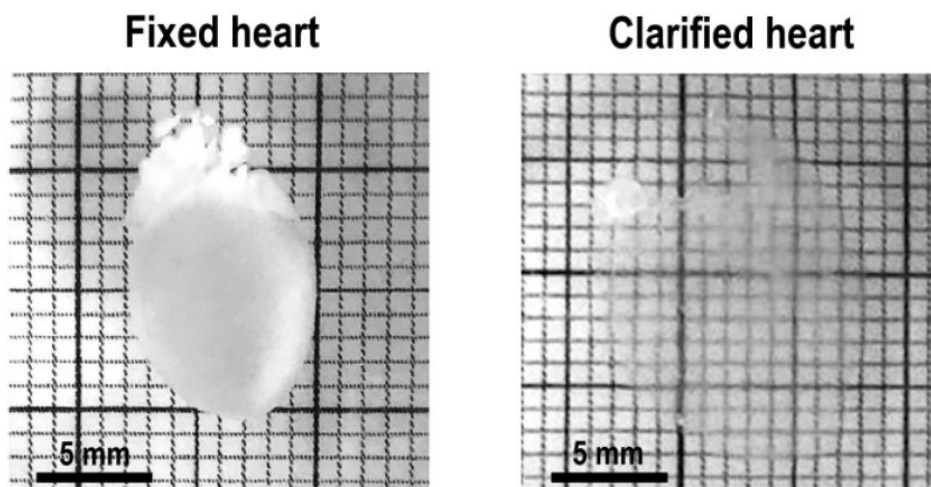


Figure 2

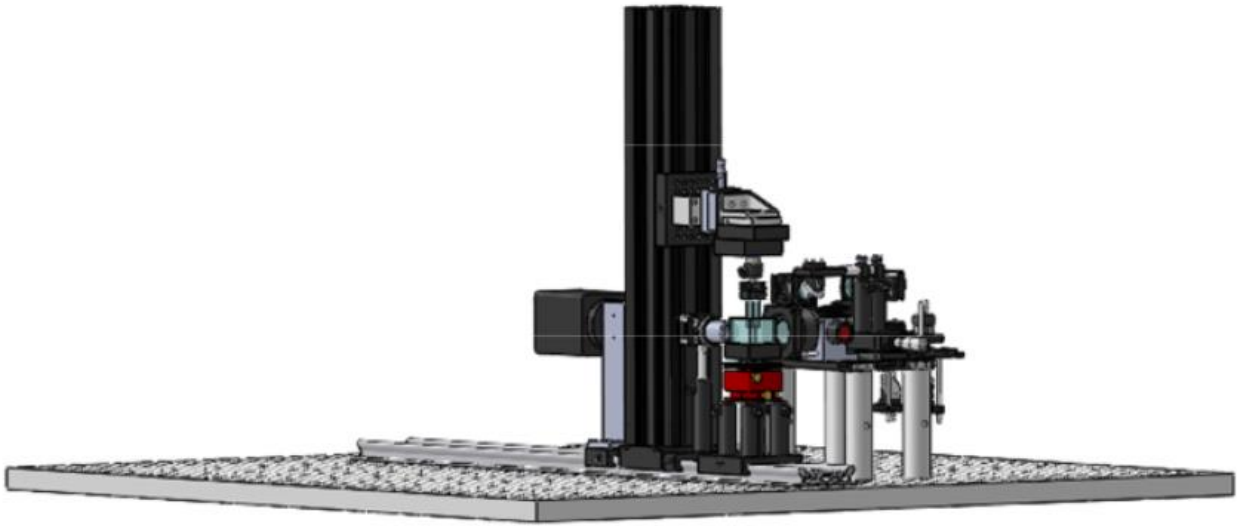


Figure 3

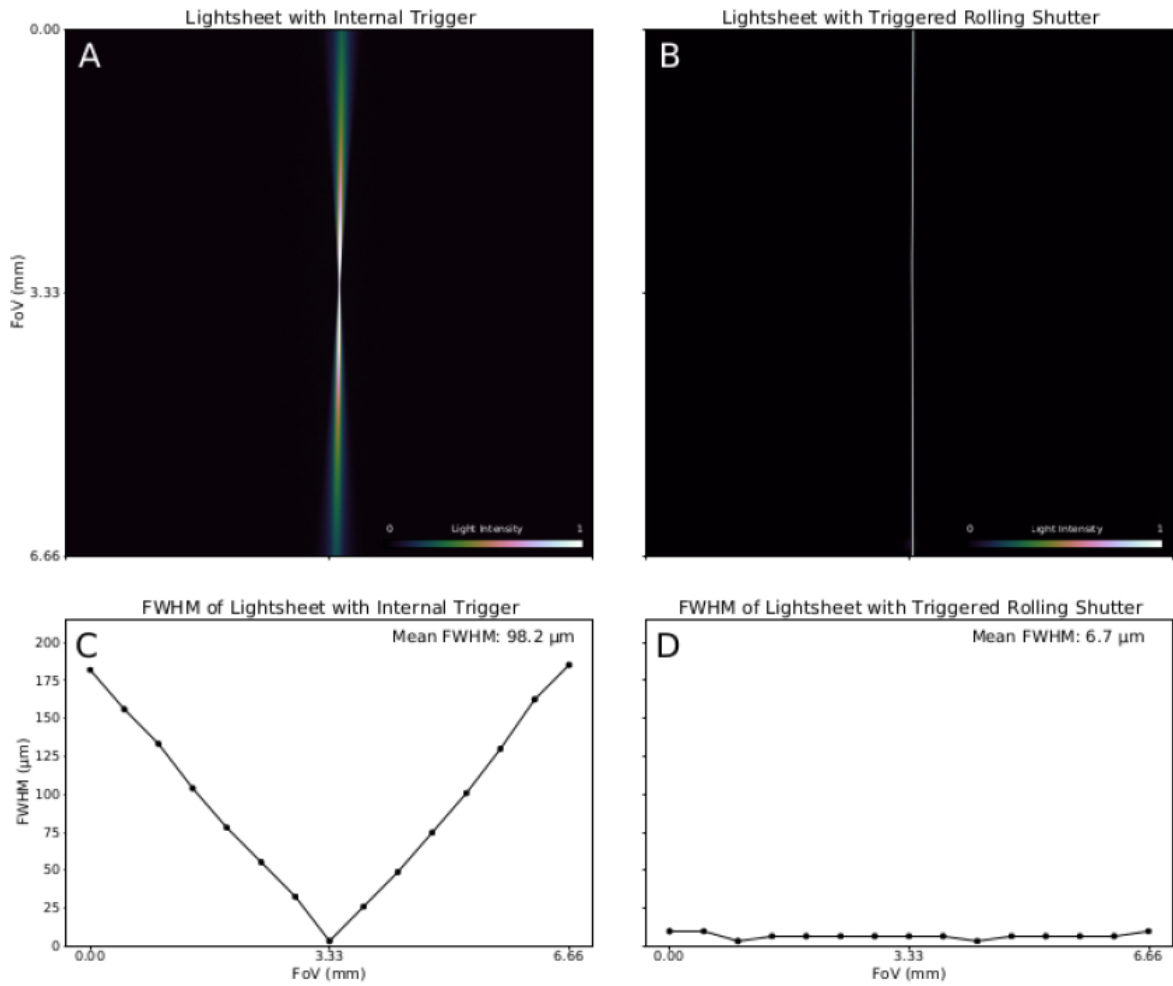


Figure 4

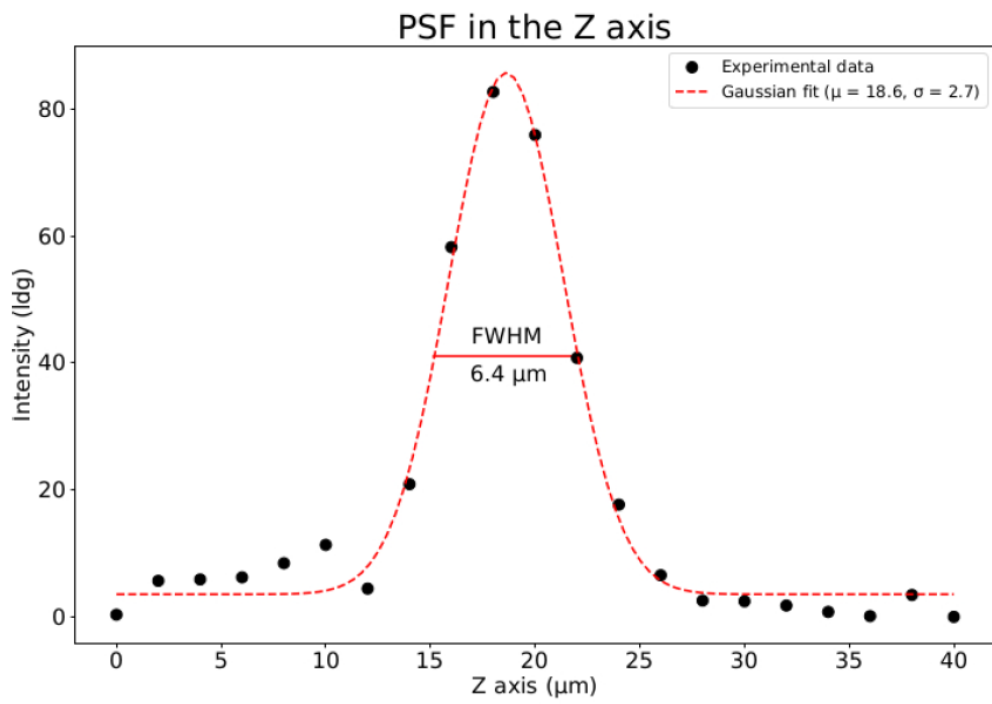


Figure 5

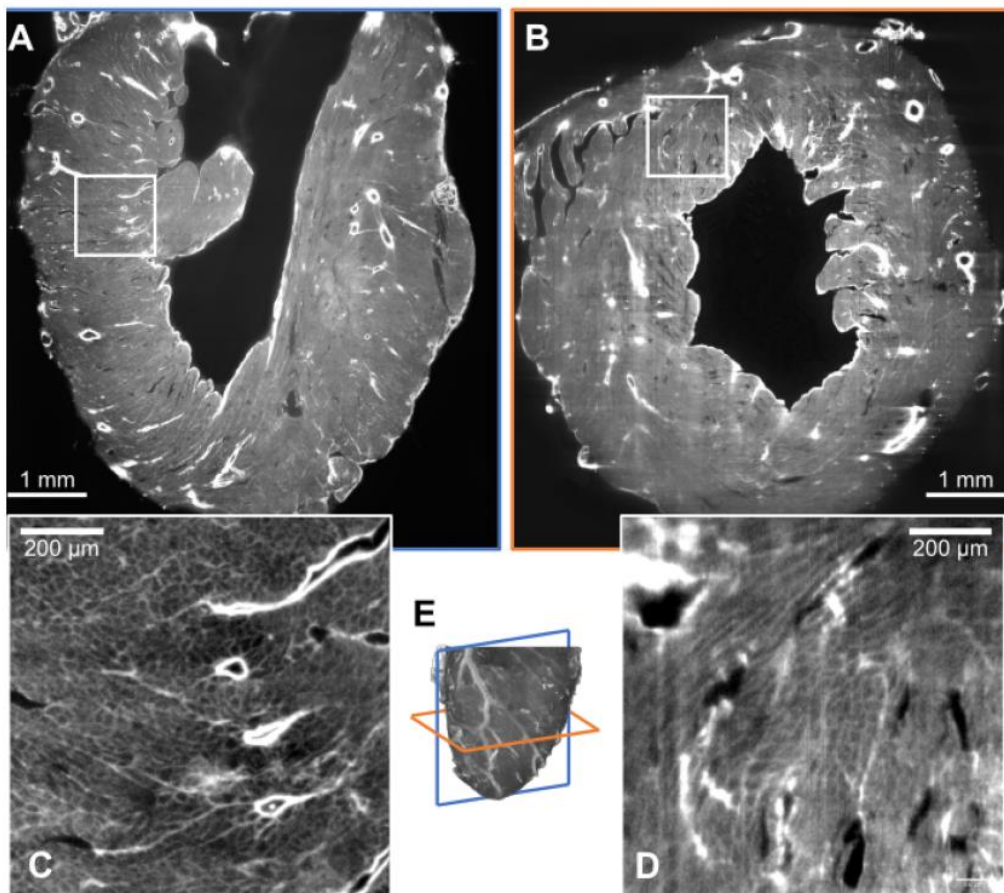


Figure 6